Sub-Hertz resonance by weak measurement

Weizhi Qu[1], Shenchao Jin[1], Jian Sun[1], Liang Jiang[2], Jianming Wen[3*], and Yanhong Xiao[1,4*]
[1]Department of Physics, State Key Laboratory of Surface Physics, and Key Laboratory of Micro and Nano Photonic Structures (Ministry of Education), Fudan University, Shanghai 200433, China
[2]Pritzker School of Molecular Engineering, University of Chicago, Chicago, Illinois 60637, USA
[3]Department of Physics, Kennesaw state University, Marietta, Georgia 30060, USA
[4]Collaborative Innovation Center of Advanced Microstructures, Nanjing 210093, China
*emails: jianming.wen@kennesaw.edu; yxiao@fudan.edu.cn.

Weak measurement (WM) with state pre- and post-selection can amplify otherwise undetectable small signals and thus promise great potentials in precision measurements. Although frequency measurements offer the hitherto highest precision owing to stable narrow atomic transitions, it remains a long-standing interest to develop new schemes to further escalate their performance. Here, we propose and demonstrate a WM-enhanced correlation spectroscopy technique which is capable of narrowing the resonance linewidth down to 0.1 Hz in a room-temperature atomic vapor cell. Potential of this technique for precision measurement is demonstrated through weak magnetic-field sensing. By judiciously pre- and post-selecting frequency-modulated input and output optical states in a nearly-orthogonal manner, a sensitivity of 7 fT/$\sqrt{\text{Hz}}$ near DC at ultralow frequency is achieved using only one laser beam of 15 μW power. Additionally, our results extend the WM framework to a non-Hermitian Hamiltonian, and shed new light on metrology and bio-magnetic field sensing applications.

Measurement is the basis for the practice of science. Being a hallmark of quantum mechanics, this assumes even a more fundamental role since the very act of measuring a system is irrevocably accompanied by a complementary disturbance. As prototypically modeled by von Neumann, the standard measurement process, in which a quantum "system" of interest is strongly coupled to an external measuring device (or "pointer") with small uncertainty, irreversibly collapses the system into an eigenstate of the Hamiltonian operator associated with the observable, and yields its corresponding eigenvalue. Contrary to this strong (projective) procedure, the notion of weak measurements (WMs) introduced by Aharonov, Albert, and Vaidman 0 describes an intriguing situation where partial information is gained by feebly probing the system without undermining its initial state. Although the uncertainty in each measurement is large because of the weak perturbative nature of the information extraction, this can be generally overcome by averaging over a vast number of identically prepared states. What makes WM an interesting phenomenon is that by post-selecting the prepared system, the weak value (WV) of an observable may lie well outside of the normal range of eigenvalues of the measurement operator, or even become complex owing to nontrivial interference effects of complex amplitudes. These peculiar features prove to be powerful for deeper understanding of quantum paradoxes and addressing important questions on the foundations of quantum mechanics [2]-[7]. Moreover, the prospect of a WV extending beyond the eigenvalue spectrum, often referred to as amplification [8], has triggered a great deal for metrological applications [9],[10] in the possibility of measuring weak signals by alleviating technical imperfections. Recently this approach has garnered substantial interest and resulted in many astounding observations in birefringence effects [11], electromagnetic pulse propagation [12], optical spin Hall effects [13], transverse beam deflections [14], phase-shift time delays [15], optical angular rotations [16], optical frequency shift [17], and optical nonlinearity at a few photon level [18], to name a few.

On the other hand, precision frequency measurements based upon atomic transitions lie at the heart of many precision measurements including atomic clocks [19] and optical magnetometry [20]. However, a major challenge is how to attain narrow linewidth ($\mathcal{L}$) but without sacrificing the measurement sensitivity, ascribed by the ratio of the linewidth to the signal-to-noise ratio (SNR). $\mathcal{L}$ is usually limited by the lifetime of

quantum states involved or the effective coherence time associated with the atom-light interaction, which gives the so called natural linewidth. Note that achieving subnatural linewidths does not violate the frequency-time uncertainty relation, as the measurement time can be much longer than the coherence lifetime [21]. Though several subnatural-linewidth spectroscopy methods [19],[22]-[27] have been put forward in the past, most of them rely crucially on (effectively) filtering out a subgroup of atoms with longer lifetime, and thus inevitably degrade the SNR by a larger factor than that of the $\mathcal{L}$-deduction. Even so, as emphasized by Metcalf and Phillips [22], narrower linewidth is still desirable especially when unknown systematic noise deforms the lineshape. Recently, a new resonance method based on measuring intensity-noise cross correlation ($g^{(2)}$) in optical fields [28]-[35] has displayed the capability of reducing the resonance linewidth far below that limited by the effective coherence lifetime by 30 times [28]. Unlike other subnatural spectroscopies [22], this method does not diminish the sensitivity [28] due to the absence of atom filtering, and can also resolve closely-spaced multiple resonance peaks [34]. Unfortunately, to date these demonstrations are restricted to large $\mathcal{L}$ about a few kHz and beyond, which has adversely locked its potentials for precision measurements.

To overcome this barrier, here we introduce the WM approach to the $g^{(2)}$-correlation spectroscopy for precise measurement of atomic resonance by properly pre- and post-selecting optical states. Due to the abnormal amplification induced by WVs, a sub-coherence-lifetime-limited $\mathcal{L}$ down to 0.1 Hz has been achieved. To demonstrate its potential applications in precision measurement, we apply it to weak magnetic field (B) sensing. In a Rb vapor cell，a sensitivity of 7 fT/$\sqrt{\text{Hz}}$ is obtained in the low frequency regime near 10-20 Hz, and less than 20 fT/$\sqrt{\text{Hz}}$ in the 20-100 Hz range. The magnetometer can be potentially used for biomagnetic field application such as the cardio-signal detections [36], if a smaller sized Cs (higher density than Rb) cell were used. To our best knowledge, previous fT-level low frequency magnetometers required high temperature (above 100℃) operation conditions [37][38][39] and this work is the realization of such sensitive near-DC magnetometers at room temperature. In addition, due to the low laser power requirement (15 μW), our magnetometer operates close to the standard quantum limit (photon shot noise) and hence allows for the future possibility of squeezed light enhanced fT-level magnetometer yet to be realized. The underlying physics process here is similar to nonlinear magneto-optical-rotation (NMOR) [40], where in contrast the measurement is performed in a different light polarization basis.

This work also exhibits a few intriguing features beyond the existing WV works, even from the theoretical perspective. For instance, instead of choosing light polarization and propagation direction as the “system” and “pointer”, our scheme exploits optical frequency and light polarization for the “system” and “pointer” respectively. We notice that although changing the dimensionality between system and pointer was utilized in the direct measurement of the quantum wavefunction [41], yet WV amplification is generally absent from that method, in contrast to our work. The frequency post-selection here gives rise to WV-amplified light polarization and a substantial reduction of $\mathcal{L}$. Although $\mathcal{L}$-reduction was achieved before in the WM on the dynamics of spontaneous emission in cold atoms [42], the frequency resolution, unexamined experimentally but only theoretically estimated, is four orders of magnitude worse than our experimental result. More strikingly, the weak interaction between the system and pointer in our scheme is intrinsically non-Hermitian and characterized by a pure imaginary Hamiltonian. Consequently, counter observations are expected as compared with conventional Hermitian Hamiltonians 0-[18]. One practical advantage of this inverse effect is the simplicity to produce an imaginary WV without designing any sophisticated interferometry setup.

Our WM protocol is performed in a generic three-level Λ-type atomic system (Fig. 1), addressed by two circularly-polarized laser fields (left-σ^+/right-σ^-) with amplitudes E_1 and E_2 (developed from one linearly-polarized cw laser) to form electromagnetically induced transparency (EIT). The two-photon detuning Δ is tuned by a B-field through offsetting the two degenerate ground states via Zeeman shift, and the information of B is carried out through the transmission of the output beams. We modulate the laser

frequency at angular frequency ω_m, and the atom-light interaction converts this frequency modulation (FM) to amplitude/intensity modulation (AM) for both EIT fields. As shown in the Supplementary Material (SM), we can derive the analytical expression of the susceptibility for σ^+ and σ^- fields from the master equation governing the atom-light interaction. We have assumed an optically thin atomic medium (verified experimentally), so that the propagation effect is neglected in our model. The relation between the input and output for the σ^+ and σ^- fields through the atomic medium of length L, in terms of their Rabi frequencies Ω_r and Ω_l, can be written as: $\begin{pmatrix}\Omega_{out,r}\\ \Omega_{out,l}\end{pmatrix} = \begin{pmatrix}\Omega_{in,r}\\ \Omega_{in,l}\end{pmatrix} e^{i\kappa L}$, where $e^{i\kappa L}$ can be treated as an evolution operator, and $\kappa = \varsigma \begin{pmatrix}\frac{\rho_r}{\Omega_{in,r}} & \\ & \frac{\rho_l}{\Omega_{in,l}}\end{pmatrix}$. The optical coherence of the atomic ensemble $\rho_{r,l}$ is a function of the ground state coherence (memory of the atomic spin) which is dependent on the laser power, giving rise to nonlinearity. Following Ref. [8], [11], [13] and [14], we can write an effective interaction Hamiltonian H for the light, with the dimension of wave vector. Yet, we note that our Hamiltonian is not a single-photon Hamiltonian as in [8], [11], [13] and [14], because in our case photons in the coherent state are not independent due to the nonlinearity. After some algebra, we arrive at the following optical Hamiltonian,

$$H = -i\xi\sigma_z \otimes (|-\omega_m\rangle\langle 0| + |\omega_m\rangle\langle 0|). \quad (1)$$

Here, $\xi = \frac{\varsigma}{\Gamma}\frac{M}{1+3M^2}\mathrm{Im}[\rho_{cb}]$ is the small, perturbative, real-valued interaction strength. $\varsigma = \frac{3N\lambda^2}{16\pi^2}\Gamma_0$ with N being the atomic density, λ the laser wavelength, and Γ_0 the spontaneous emission rate of the excited state. $M = \frac{\lambda_m\omega_m}{\Gamma}$, with Γ being the Doppler broadened linewidth of the excited state, λ_m the modulation depth. $\mathrm{Im}[\rho_{cb}]$ is the imaginary part of the ground state coherence ρ_{cb} of the atoms, which is proportional to Δ and is a function of the laser intensity (see SM). It can be seen that the faster the modulation, the smaller the atomic response. The "pointer" operator $\sigma_z = \begin{pmatrix}1 & 0\\ 0 & -1\end{pmatrix}$ assumes the eigenvalue of $+1$ or -1 when acting on the corresponding σ^+-eigenvector $\begin{pmatrix}1\\0\end{pmatrix}$ or the σ^--eigenvector $\begin{pmatrix}0\\1\end{pmatrix}$, respectively. By projecting onto the final state, the expectation value $\langle\sigma_z\rangle$ quantifies the intensity difference, thus the absorption difference between the transmitted σ^+ and σ^- fields. The "system" operator is the frequency operator $|-\omega_m\rangle\langle 0| + |\omega_m\rangle\langle 0|$ acting on the Hilbert space that contains three frequency components: $|-\omega_m\rangle$, $|\omega_m\rangle$ and $|0\rangle$, and is in the rotating frame defined by the modulated laser frequency. It describes the FM-AM conversion. As usual, the frequency vector here obeys the condition $\langle\omega_i|\omega_j\rangle = \delta(\omega_i - \omega_j)$. We note that because the second and higher harmonics are much smaller compared to the first harmonics in the AM, they are neglected in H. Distinct fundamentally from traditional WM Hamiltonians, the presence of "i" in H here reveals the anti-Hermitian nature of the interaction owing to the differential absorption for σ^+ and σ^- fields.

The Hamiltonian (1) shows that the frequency and the polarization of the light are correlated due to the atom-light interaction. For example, for the DC component of the two laser intensities, σ_z is zero for any magnetic field B. However, the AC component of the σ_z at ω_m is nonzero and is proportional to the magnetic field B (for B). This suggests that one can do post-selection in the frequency domain to enhance the signal. In light of the WM procedure, the atoms are illuminated by an x-polarized cw laser with the initial state prepared as a product of the "pointer" and the "system": $|\Psi_i\rangle = |\Phi_{pi}\rangle \otimes |\Psi_{si}\rangle = \frac{1}{\sqrt{2}}\begin{pmatrix}1\\1\end{pmatrix} \otimes |0\rangle$. After traversing the atomic medium of length L, the final output optical state is $|\Psi_f\rangle \approx (1 - iHL)|\Psi_i\rangle$. By post-selecting the output "system" state $|\Psi_{sf}\rangle$ which is nearly orthogonal to $|\Psi_{si}\rangle = |0\rangle$, the polarization state of the output light $|\Phi_{pf}\rangle = \langle\Psi_{sf}|\Psi_f\rangle$ is then obtained by tracing out the "system". Here, $|\Psi_{sf}\rangle = \frac{1}{\sqrt{(1-D)^2+2}}[(1-D)|0\rangle + |\omega_m\rangle + |-\omega_m\rangle]$ is formed by the central frequency component superposed by the first side-bands, with D the post-selection parameter very close to unity. Alternatively, one can show that this post-selection operation is equivalent to subtracting the majority of the DC component of the

transmitted light power while retaining the AC components. The asymmetric forms of $|\Psi_{si}\rangle$ and $|\Psi_{sf}\rangle$ are also opposed to the symmetric ones often considered in previous WV-amplification experiments [9]-[18]. After normalization, $|\Phi_{pf}\rangle$ becomes

$$|\Phi_{pf}\rangle = (1 - \xi L A_W \sigma_z)|\Phi_{pi}\rangle \approx e^{-\xi L A_W \sigma_z}|\Phi_{pi}\rangle. \quad (2)$$

Here, the WV associated with the system observable is defined as

$$A_W = \frac{\langle\Psi_{sf}|(|-\omega_m\rangle\langle 0|+|\omega_m\rangle\langle 0|)|\Psi_{si}\rangle}{\langle\Psi_{sf}|\Psi_{si}\rangle} = \frac{2}{1-D}, \quad (3)$$

which is a real quantity. It is worth pointing out that in spite of the real A_W, the anti-Hermiticity of the interaction Hamiltonian (1) makes the results equivalent to the imaginary WV obtained from a Hermitian one. So far, most of imaginary WV realizations are indispensable to sophisticated interferometric systems. By constructing a non-Hermitian Hamiltonian, our scheme grants an alternative way without the complexity of experimental setups. With $|\Phi_{pf}\rangle$, one can now readily have $\langle\sigma_z\rangle_{pf} = -2\xi L A_W$, indicating the WV-amplified Stokes parameter.

Now, we establish the relation between $\langle\sigma_z\rangle$ and the WM-$g^{(2)}(0)$ spectroscopy, and derive the resonance linewidth $\mathcal{L}$. The measured quantity here is the second-order correlation function between the two EIT fields' output intensities at the zero-time lag, $g^{(2)}(0) = \langle I_1(t)I_2(t)\rangle/\sqrt{\langle I_1^2(t)\rangle\langle I_2^2(t)\rangle}$ (see Methods), which is a function of $B(\propto \Delta)$. Since $g^{(2)}(0)$ is bounded between -1 and 1 corresponding to anti-correlation and correlation between the two intensities, $\mathcal{L}$ can be deduced by simply seeking the zero-value of $g^{(2)}(0)$. Since $\langle\sigma_z\rangle$ corresponds to intensity difference between σ^+ and σ^- and it only has a nonzero AC component proportional to Δ, the larger the AC-component of $\langle\sigma_z\rangle$, the larger the anti-correlation signal (Fig.1), and the closer is $g^{(2)}(0)$ to -1. On the other hand, the DC component in the σ^+ and σ^- intensities contributes to correlation with a strength proportional to $(1 - D)$. If D is larger, the correlated component becomes smaller, so the anti-correlated needs to be smaller to let $g^{(2)}(0) = 0$, which means a smaller Δ and consequently a reduced $\mathcal{L}$. We can also rigorously prove that $\langle I_1(t)I_2(t)\rangle$ is interlinked with the Stokes parameter $\langle\sigma_z\rangle$ (see SM). For standard measurements, $\langle\sigma_z\rangle$ satisfies the inequality $\langle\sigma_z\rangle \leq 1$. On the contrary, the condition of $g^{(2)}(0) = 0$ demands $\langle\sigma_z\rangle = \sqrt{2}$, in opposition to the inequality. It turns out that the WV amplification of $\langle\sigma_z\rangle$, as derived above, makes this possible. Consequently, the $g^{(2)}(0)$ linewidth becomes $\mathcal{L} = \frac{\sqrt{2}}{\left|L\left(\frac{\partial\xi}{\partial\Delta}\right)A_W\right|}$, suggesting the anomalous WV-induced narrowing.

When assessing the frequency resolution of the WM-$g^{(2)}(0)$ spectroscopy, one has to take into account the SNR in addition to the linewidth. As will become clear, this subnatural-$\mathcal{L}$ spectroscopy is distinct from most line-narrowing techniques in that the $\mathcal{L}$-reduction does not sacrifice the frequency resolving power. Under the current WM arrangement, the ultimate SNR, only limited by the photon shot noise (see Methods), follows the trend of $\frac{2\sqrt{2}}{A_W}\sqrt{n_{\mathrm{ph}}}$ with n_{ph} being the total photon-number rate (see SM). Because both $\mathcal{L}$ and SNR are inversely proportional to A_W, the ultimate frequency resolving power defined by their ratio has nothing to do with A_W, agreeing with the fact that classical experiments cannot breach the quantum limit. Nevertheless, the WM strategy helps to eliminate adverse effect from technical imperfections [43].

In the experiment as schematically shown in Fig. 1, a linearly polarized optical beam was derived from an external cavity diode laser, and then directed into a ^{87}Rb enriched cylindrical atomic vapor cell (2 cm in diameter and 7.1 cm in length) at room temperature (~22°C). With alkene coating [44], the cell was housed inside a four-layer μ-metal magnetic shield to screen out ambient field. The alkene coating allows atoms to undergo thousands of wall collisions with little demolition of their internal quantum states, thus giving a deduced zero-power EIT half linewidth of 1 Hz (dominated by decoherence from the ambient B field inhomogeneities). Inside the shield, a solenoid was used to generate a uniform B-field along the laser's

propagation direction, and two-photon detuning Δ was introduced through Zeeman shift. The input laser, on resonance with the ^{87}Rb D_1 line (795 nm), drives the atomic transitions $|F=2\rangle \rightarrow |F'=1\rangle$ with its two circular-polarization components, σ^+ and σ^-, to form EIT. Their outputs were separately detected by two photo-detectors with gain for analyzing their fluctuating intensities. The laser frequency was modulated at an optimized modulation frequency of 3.03 kHz, with a modulation range of 250 MHz, by varying the PZT voltage. The residual amplitude modulation (RAM) and laser intensity noise were reduced by a feedback loop controlling the RF power of an acoustic-optic modulator in the light stream before the cell. Upon interacting with the atoms, the laser frequency modulation was converted into intensity modulation. We have experimentally verified the optical depth (OD) by measuring the transmission of the light off two-photon resonance but on one-photon resonance, and found that OD~0.21, indicating an optically thin regime.

After recording the intensity outputs of the σ^+ and σ^- fields simultaneously by two individual photo-detectors, we perform fast Fourier transform (FFT) and digital filtering to pick out the frequency component at ω_m, as well as the DC part. We next apply numerically an attenuation factor $(1-D)$ to the DC component, where D is the post-selection parameter and can be optimized for the best magnetometer sensitivity. Then, the two intensity signals (in the temporal domain) for σ^+ and σ^-, containing the AC components at ω_m and the attenuated DC component, are used to compute the value of $g^{(2)}(0)$. The FFT is done for in each modulation period and one $g^{(2)}(0)$ data point is produced. Alternatively, the amplitude and the phase of the AC components described above could be obtained using a two-channel lock-in amplifier.

We first investigate $\mathcal{L}$ as a function of the post-selection parameter D. With optimized modulation range and laser power, we can obtain the $g^{(2)}(0)$ resonance spectrum with a half width at half maximum (HWHM) of 0.1 Hz for $D=0.9995$, as shown in Fig. 2a. This linewidth is ten times smaller than the coherence-lifetime-limited width of 1 Hz, and 130 times narrower than the power-broadened EIT linewidth 13 Hz for 15 μW operation laser power. Here each $g^{(2)}(0)$ value is acquired in one modulation period ($T=2\pi/\omega_m$). As one can see, the $g^{(2)}(0)$ spectrum, displaying full correlation and anti-correlation, is well fitted by a Lorentzian profile as predicted by our theory (see SM). The linear dependence of $\mathcal{L}$ on D was also well confirmed in Fig. 2b, where $\mathcal{L}$ monotonically decreases with larger D. In the experiment, we found that $\mathcal{L}$ can be further reduced by increasing D but with worse SNR, and the $g^{(2)}(0)$ resonance spectrum also deviates from the Lorentzian lineshape. Intuitively, as D approaches one, the correlated DC component in the outputs nearly vanishes; whilst noises such as laser intensity noise become dominant and yield fluctuating correlation signals, resulting in the SNR drop.

We next use this WM-$g^{(2)}(0)$ resonance for weak B-field sensing. Before proceeding, we emphasize that, in addition to magnetometry, our correlation resonance technique, as a very sensitive spectroscopy, is applicable to resolving closely spaced multi-resonance peaks and other precision measurements [45][46]. To experimentally probe the magnetometer sensitivity, we apply a weak DC magnetic field corresponding to $g^{(2)}(0)\simeq 0$ where the resonance slope is large. As illustrated in Fig. 3 and in the SM, our magnetometer is sensitive to low-frequency B-fields, up to ~200 Hz. The magnetometer bandwidth is determined by the optical pumping rate. In particular, the best sensitivity of 7 fT/$\sqrt{\text{Hz}}$ falls in the 10 ~ 20 Hz range, with the post-selection parameter $D=0.995$. This D value corresponds to a half width of ~1 Hz for the $g^{(2)}(0)$ profile, much smaller than the power-broadened EIT resonance linewidth of 13 Hz. The optimization of D for the best B sensitivity turns out to be a trade-off between $\mathcal{L}$ and SNR: although small $\mathcal{L}$ requires large D, in presence of technical noises, yet a larger D could adversely aggravate the effect of technical noise on the $g^{(2)}(0)$ value and result in drastic reduction on SNR (see Methods). With an overall sensitivity below 10 fT/$\sqrt{\text{Hz}}$ in the range of 5 ~ 40 Hz, and 20 fT/$\sqrt{\text{Hz}}$ up to 100Hz (see SM), this magnetometer is suitable for low-frequency B-field sensing. The room temperature and low laser-power operation conditions make our scheme attractive for practical applications [47].

Finally, we investigate the advantages of the WM-$g^{(2)}(0)$ approach for magnetomtery in presence of various noise sources, when compared to other measurement techniques. As stated above, WM cannot break the quantum limit in spite of the line narrowing effect, but it can alleviate adverse effects of technical noise on the sensitivity by engineering the overlap between the initial and final "system" states. Firstly, we study how the post-selection parameter D affect the sensitivity. In our FM experiment, the laser intensity noise including RAM, is a typical noise source that contributes to positive correlation, affecting both the signal level and the noise of $g^{(2)}(0)$, as derived in the SM. To investigate its effects in a controllable way, we have designed a feedback loop to reduce the RAM level by 25 dB, and instead added common-mode random white-intensity-noise at the two outputs to mimic RAM and laser intensity noise. Similar to previous WM research, the sensitivity becomes worse when $|\Psi_{si}\rangle$ and $|\Psi_{sf}\rangle$ are almost orthogonal (i.e. $D \approx 1$), because technical noises overwhelm signal. As shown in Fig. 4, the sensitivity degrades drastically as D approaches one, and it also gradually becomes worse with increasing RAM. However, when $D \leq 0.98$, the RAM does not affect sensitivity substantially as the projected DC component in intensity dominates over the noises. Secondly, we compared our scheme with the traditional lock-in detection [48] which usually only uses the AC signal and is here represented by the intensity-difference method, i.e., taking the intensity difference of σ^+ and σ^- at frequency ω_m. For impure input linear polarization along with RAM, we found the WM-$g^{(2)}(0)$ method can outperform the direct intensity-difference measurement for proper D settings, as the WM-$g^{(2)}(0)$ is more immune to the RAM noise (see Fig. 5). When no RAM exists, although these two methods yield the same sensitivity, the WM-$g^{(2)}(0)$ scheme is still superior in producing much narrower resonance linewidth for spectroscopy; whereas the intensity difference method gives normal power-broadened linewidth. Thirdly, unlike NMOR where the polarization rotation of the input light is measured, i.e., the phase difference between the two circular light components [40][48], in our work we measure the intensity difference between them. Such selection of measurement basis becomes advantageous when there is quantum backaction noise (see Methods), a factor preventing some resonant magnetometers from reaching the photon-shot-noise limited sensitivity [40][48].

In short, we have used WV amplification to narrow the $g^{(2)}(0)$-resonance linewidth in a warm ^{87}Rb vapor well below that limited by the coherence lifetime. The scheme exhibits a number of intriguing features, including the selections of "system" and "pointer" for the weak measurement, the anti-Hermiticity of the interaction Hamiltonian, and the ingenious relation between the Stokes parameter and the $g^{(2)}(0)$ measurement. The simplicity, low power consumption, and good sensitivity of the WM-$g^{(2)}(0)$ based magnetometer makes it promising for real applications in the low frequency magnetic fields. Despite one drawback is to sacrifice the dynamical range for detectable magnetic field, this could be overcome by using two EIT fields with frequency offset equal to the Larmor frequency. As a novel subnatural spectroscopy method, this approach is useful for determining resonance center as emphasized in [22]. Furthermore, this resonance scheme belongs to the broad category of noise-correlation spectroscopy which is deemed to hold potential in other precision measurement applications such as detecting low energy modes [45] and optical forces [46] in cold atoms. Future development of this technique may incorporate quantum enhancement by including squeezed light or squeezed atomic spin [50].

References

[1] Aharonov, Y., Albert, D. Z. & Vaidman, L. How the result of a measurement of a component of the spin of a spin-1/2 particle can turn out to be 100. *Phys. Rev. Lett.* **60**, 1351-1354 (1988).

[2] Kocsis, S., Braverman B., Ravets S., Stevens M. J., Mirin, R. P., Shalm, L. K. & Steinberg, A. M. Observing the average trajectories of single photons in a two-slit interferometer. *Science* **332**, 125-131 (2011).

[3] Lundeen, J. S., Sutherland, B., Patel, A., Stewart, C. & Bamber, C. Direct measurement of the quantum wavefunction. *Nature* **474**, 188-191 (2011).

[4] Lundeen, J. S. & Steinberg, A. M. Experimental joint weak measurement on a photon pair as a probe of Hardy's paradox. *Phys. Rev. Lett.* **102**, 020404 (2009).
[5] Yokota, K., Yamamoto, T., Koashi, M. & Imoto, N. Direct observation of Hardy's paradox by joint weak measurement with an entangled photon pair. *New J. Phys.* **11**, 033011 (2009).
[6] Kim, Y.-S., Lee, J.-C., Kwon, O. & Kim, Y.-H. Protecting entanglement from decoherence using weak measurement and quantum measurement reversal. *Nat. Phys.* **8**, 117-120 (2012).
[7] Wu, S. & Żukowski, M. Feasible optical weak measurements of complementary observables via a single Hamiltonian. *Phys. Rev. Lett.* **108**, 080403 (2012).
[8] Duck, I. M., Stevenson, P. M. & Sudarshan, E. C. G. The sense in which a "weak measurement" of a spin-1/2 particle's spin component yields a value 100. *Phys. Rev. D* **40**, 2112-2117 (1989).
[9] Dressel, J., Malik, M., Miatto, F. M., Jordan, A. N. & Boyd, R. W. Understanding quantum weak values: Basics and applications. *Rev. Mod. Phys.* **86**, 307-316 (2014).
[10] Kofman, A. G., Ashhab, S. & Nori, F. Nonperturbative theory of weak pre- and post-selected measurements. *Phys. Rep.* **520**, 43-133 (2012).
[11] Ritchie, N. W. M., Story, J. G. & Hulet, R. G. Realization of a measurement of a "weak value". *Phys. Rev. Lett.* **66**, 1107-1110 (1991).
[12] Solli, D. R., McCormick, C. F., Chiao, R. Y., Popescu, S. & Hickmann, J. M. Fast light, slow light, and phase singularities: A connection to generalized weak values. *Phys. Rev. Lett.* **92**, 043601 (2004).
[13] Hosten, O. & Kwiat, P. Observation of the spin Hall effect of light via weak measurements. *Science* **319**, 787-790 (2008).
[14] Dixon, P. B., Starling, D. J., Jordan, A. N. & Howell, J. C. Ultrasensitive beam deflection measurement via interferometric weak value amplification. *Phys. Rev. Lett.* **102**, 173601 (2009).
[15] Brunner, N. & Simon, C. Measuring small longitudinal phase shifts: Weak measurements or standard interferometry? *Phys. Rev. Lett.* **105**, 010405 (2010).
[16] Magaňa-Loaiza, O. S., Mirhosseini, M., Rodenburg, B. & Boyd, R. W. Amplification of angular rotations using weak measurements. *Phys. Rev. Lett.* **112**, 200401 (2014).
[17] Starling, D. J., Dixon, P. B., Jordan, A. N. & Howell, J. C. Precision frequency measurements with interferometric weak values. *Phys. Rev. A* **82**, 063822 (2010).
[18] Hallaji, M., Feizpour, A., Dmochowski, G., Sinclair, J. & Steinberg, A. M. Weak-value amplification of the nonlinear effect of a single photon. *Nat. Phys.* **13**, 540-544 (2017).
[19] Godone, A., Levi, F. & Micalizio, S. Subcollisional linewidth observation in the coherent-population-trapping Rb maser. *Phys. Rev. A* **65**, 031804(R) (2002).
[20] Budker, D. & Kimball, D. F. J. *Optical Magnetometry* (Cambridge University Press, UK, 2013).
[21] Busch, P. in *Time in Quantum Mechanics* edited by Muga, J. G., Sala Mayato, R. & Egusquiza, I. L. (Springer-Verlag, Berlin, 2008), pp. 73-105.
[22] Metcalf, H. & Phillips, W. Time-resolved subnatural-width spectroscopy. *Opt. Lett.* **5**, 540-542 (1980).
[23] Knight, P. L. & Coleman, P. E. Subnatural linewidth spectroscopy. *J. Phys. B* **13**, 4345-4352 (1980).
[24] Lee, H. W., Meystre, P. & Scully, M. O. Theory of time-delayed measurement: Subnatural linewidth and transient dip spectroscopy. *Phys. Rev. A* **24**, 1914-1924 (1981).
[25] Dugan, M. A. & Albrecht, A. C. Radiation-matter oscillations and spectral line narrowing in field-correlated four-wave mixing. II. Experiment. *Phys. Rev. A* **43**, 3922-3933 (1991).
[26] Hald, J., Petersen, J. C. & Henningsen, J. Saturated optical absorption by slow molecules in hollow-core photonic band-gap fibers. *Phys. Rev. Lett.* **98**, 213902 (2007).
[27] Lam, J. F., Steel, D. G. & McFarlane, R. A. Observation of collision-induced subnatural Zeeman-coherence linewidths in the Doppler limit. *Phys. Rev. Lett.* **56**, 1679-1682 (1986).

[28] Feng, L., Li, P., Jiang, L., Wen, J. & Xiao, Y. Coherence-assisted resonance with sub-transit-limited linewidth. *Phys. Rev. Lett.* **109**, 233006 (2012).
[29] Xiao, Y., Wang, T., Baryakhtar, M., Van Camp, M., Crescimanno, M., Hohensee, M., Jiang, L., Phillips, D. F., Lukin, M. D., Yelin, S. F. & Walsworth, R. L. Electromagnetically induced transparency with noisy lasers. *Phys. Rev. A* **80**, 041805(R) (2009).
[30] Sautenkov, V. A., Rosovtsev, Y. V. & Scully, M. O. Switching between photon-photon correlations and Raman anticorrelations in a coherently prepared Rb vapor. *Phys. Rev. A* **72**, 065801 (2005).
[31] Ariunbold, G. O., Rostovtsev, Y. V., Sautenkov, V. A. & Scully, M. O. Intensity correlation and anti-correlations in coherently driven atomic vapor. *J. Mod. Opt.* **57**, 1417-1427 (2010).
[32] Cruz, L. S., Felinto, D., Gomez, J. G. A., Martinelli, M., Valente, P., Lezama, A. & Nussenzveig, P. Laser-noise-induced correlations and anti-correlations in electromagnetically induced transparency. *Eur. Phys. J. D* **41**, 531-539 (2006).
[33] Felinto, D., Curz, L. S., de Oliveira, R. A., Florez, H. M., de Miranda, M. H. G., Nussenzveig, P., Martinelli, M. & Tabosa, J. W. R. Physical interpretation for the correlation spectra of electromagnetically-induced-transparency resonances. *Opt. Express* **21**, 1512-1519 (2013).
[34] Li, P., Feng, L. & Xiao, Y. Resolving multiple peaks using a sub-transit-linewidth cross-correlation resonance. *Phys. Rev. A* **89**, 043825 (2014).
[35] Zheng, A., Green, A., Crescimanno, M. & O'Leary, S. Electromagnetically-induced-transparency intensity-correlation power broadening in a buffer gas. *Phys. Rev. A* **93**, 043825 (2016).
[36] Groeger, S., Bison, G., Knowles, P. E., Wynands, R., Weis A., Laser-pumped cesium magnetometers for high-resolution medical and fundamental research. *Sensors and Actuators A* **129**, 1-5 (2006).
[37] Dang, H. B., Maloof, A. C. & Romalis, M. V. Ultrahigh sensitivity magnetic field and magnetization measurements with an atomic magnetometer. *Appl. Phys. Lett.* **97**, 151110 (2010).
[38] Kominis, I. K., Kornack, T. W., Allred, J. C. & Romalis, M. V. A subfemtotesla multichannel atomic magnetometer. *Nature* **422**, 596-599 (2003).
[39] Jiang, M., Wu, T., Blanchard, J. W., Feng, G., Peng, X. & Budker, D. Experimental benchmarking of quantum control in zero-field nuclear magnetic resonance. *Sci. Adv.* **4** :eaar6327 (2018).
[40] Ledbetter, M. P., Acosta, V. M., Rochester, S. M., Budker, D., Pustelny, S. & Yashchuk, V. V. Detection of radio-frequency magnetic fields using nonlinear magneto-optical rotation. *Phys. Rev. A* **75**, 023405 (2007).
[41] Vallone, G. & Dequal, D. Strong Measurements Give a Better Direct Measurement of the Quantum Wave Function. *Phys. Rev. Lett.* **116** 040502 (2016)
[42] Shomroni, I., Bechler, O., Rosenblum, S. & Dayan, B. Demonstration of Weak Measurement Based on Atomic Spontaneous Emission. *Phys. Rev. Lett.* **111**, 023604 (2013).
[43] Jordan, A. N., Martínez-Rincón, J. & Howell, J. C. Technical Advantages for Weak-Value Amplification: When Less Is More. *Phys. Rev. X* **4**, 011031(2014).
[44] Balabas, M. V., Karaulanov, T., Ledbetter, M. P. & Budker, D. Polarized alkali-metal vapor with minute-long transverse spin-relaxation time. *Phys. Rev. Lett*. **105**, 070801 (2010).
[45] Sparapassi, G., Tollerud, J. O., Glerean, F. & Fausti, D. Noise Correlation Spectroscopy for spectroscopic measurements of low energy modes, in Conference on Lasers and Electro-Optics, OSA Technical Digest (online) (Optical Society of America, 2018), paper ATh3O.7.
[46] Theophilo, K., Kumar, A., Florez, H. M., González-Arciniegas, C., Nussenzveig, P. & Martinelli, M. Probing light forces on cold atoms by noise correlation spectroscopy. *Phys. Rev. A* **98**, 053832 (2018).
[47] Schiwindt, P. D. D., Knappe, S., Shah, V., Hollberg, L., Kitching, J., Liew, L.-A. & Moreland, J. Chip-scale atomic magnetometer. *Appl. Phys. Lett.* **85**, 6409-6411 (2004).

[48] Bjorklund, G. C., Levenson, M. D., Lenth, W. & Ortiz, C. Frequency modulation (FM) spectroscopy-theory of lineshapes and signal-to-noise analysis. *Appl. Phys. B* **32**, 145-152 (1983).
[49] Novikova, I., Mikhailov, E., & Xiao, Y. Excess optical quantum noise in atomic sensors. *Phys. Rev. A* **91**, 051804(R) (2015).
[50] Bao, H., Duan, J., Lu, X., Li, P., Qu, W., Jin, S., Wang, M., Novikova, I., Mikhailov, E., Zhao, K. -F., Mølmer, K., Shen, H., & Xiao, Y. Measurements with prediction and retrodiction on the collective spin of 10^{11} atoms beat the standard quantum limit. *arXiv*:1811.06945 (2018).

Acknowledgements
We are grateful to Irina Novikova, Eugeniy Mikhailov, Kaifeng Zhao, Dong Sheng, Heng Shen, Shengjun Wu and Lijian Zhang for helpful discussions. This work is supported by National Key Research Program of China under Grant Nos. 2016YFA0302000 and 2017YFA0304204, and NNSFC under Grant No. 61675047 and 91636107. L.J. acknowledged funding supports from the ARL-CDQI (W911NF-15-2-0067, W911NF-18-2-0237), AFOSR MURI (FA9550-14-1-0052), DOE (DE-SC0019406), NSF (EFMA-1640959), and the Packard Foundation (2013-39273). J.W. was supported by the NSF EFMA-1741693, NSF 1806519, and Kennesaw State University.

Author contributions
Y.X., W.Q. and J.W. conceived the idea. J.S. and S.J. performed the experiment. The theoretical derivation was performed by W.Q. with supervision from J.W, L.J. and Y.X. Y.X. and J.W. wrote the manuscript with contributions from all other authors. All contributed to the discussion of the project and analysis of experimental data. Y.X. supervised the project.

Additional information
Supplemental information is available in the online version of the paper. Reprints and permissions information is available online. Correspondence and requests for materials should be addressed to Y.X. or J.W.

Competing financial interests
The authors declare no competing financial interests.

List of Figures

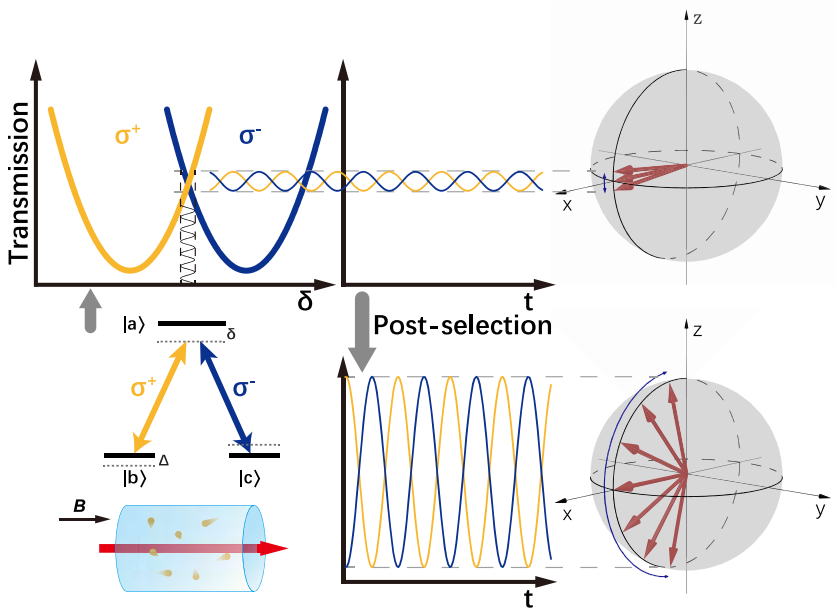

Figure 1 | Principle and schematics of WM-enhanced correlation spectroscopy. The σ^+ and σ^- circular components of a linearly polarized laser beam form EIT with the atoms under a three-level Λ configuration. The transmission spectra of σ^+ and σ^- overlap when the two-photon-detuning $\Delta = 0$, but splits when $\Delta \neq 0$. The offset spectra give opposite transmission slopes for σ^+ and σ^- around $\delta = 0$, responsible for the out-of-phase FM-AM conversion and the anti-correlation. The converted intensity modulations correspond to a small oscillation of the Stokes vector of light on the Poincaré sphere, and the oscillation amplitude is proportional to Δ. By post-selecting frequency components of the two EIT fields, an anomalous amplification of the oscillation can be achieved, giving rise to reduction of the correlation resonance linewidth (see text). Here, δ is the averaged one-photon detuning, and Δ is the two-photon detuning due to Zeeman shifts on energy levels caused by the total magnetic field B.

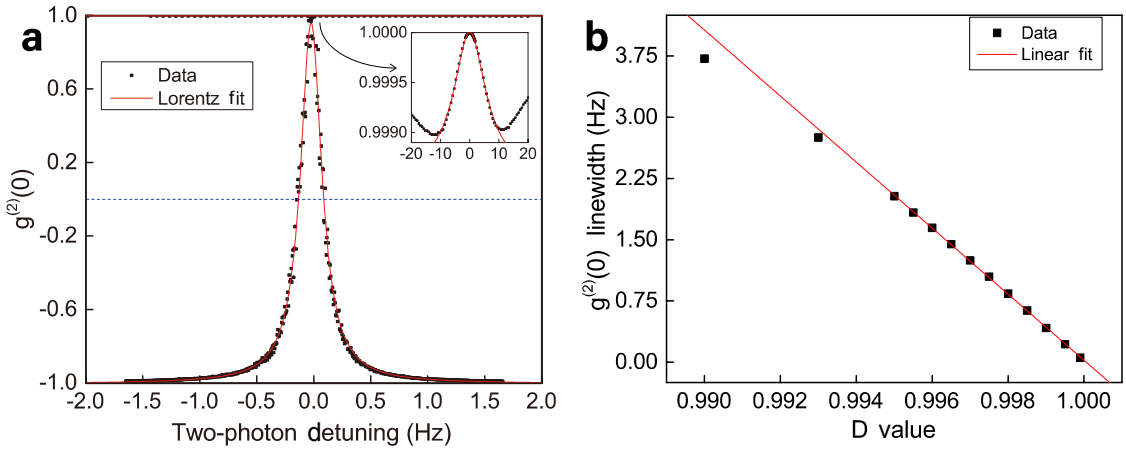

Figure 2 | Representative correlation-resonance spectrum of $g^{(2)}(0)$ and its linewidth $\mathcal{L}$ behavior. **a**, Exemplar of the $g^{(2)}(0)$-resonance spectral profile with the HWHM of about 0.1 Hz, ten times smaller than the coherence-lifetime-limited half width of ~1 Hz, obtained by setting $D = 0.9995$. As a comparison, the inset displays the corresponding spectrum without post-selection ($D = 0$). The "two-photon detuning" of the x-axis is equal to the relative Zeeman shift of the ground state energy levels, and is proportional to the total magnetic field including the residual stray field inside the shield and the applied magnetic field to be measured. **b**, Linear dependence of the full width at half maximum (FWHM) of $g^{(2)}(0)$-resonance on the projection parameter D, for an input x-polarized cw laser of power 15 μW, in good agreement with the trend predicted by our theory.

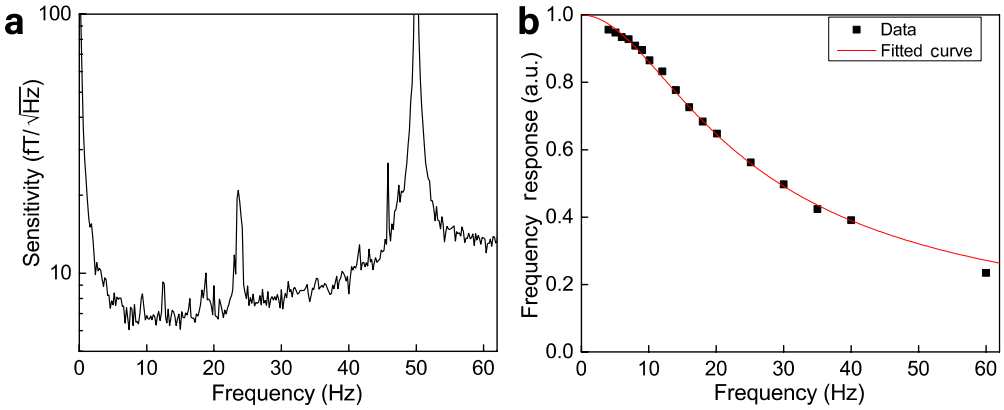

Figure 3 | Sensitivity and frequency response of the magnetometer based on WM-$g^{(2)}(0)$ resonance. **a**, The sensitivity spectrum derived from the $g^{(2)}(0)$ noise spectrum divided by the "resonance slope vs. frequency" curve. The former was generated by Fourier transform of 30300 continuous data points of $g^{(2)}(0)$ values measured at $g^{(2)}(0)\sim 0$, within 10 seconds, with each data point obtained from one modulation period. **b**, The normalized $g^{(2)}(0)$ resonance slope measured at $g^{(2)}(0)\sim 0$ for various AC magnetic field frequencies, with respect to the slope measured for a DC magnetic field. The fitting curve follows the function $BW/\sqrt{BW^2 + f^2}$ with $BW = 16$ Hz. Experimental parameters: laser power of 15 μW and $D = 0.995$. The test DC field we applied is 0.1 nT for assessing the magnetometer sensitivity. The magnitude of the oscillating magnetic field for measuring the atomic frequency response is 3.9 pT.

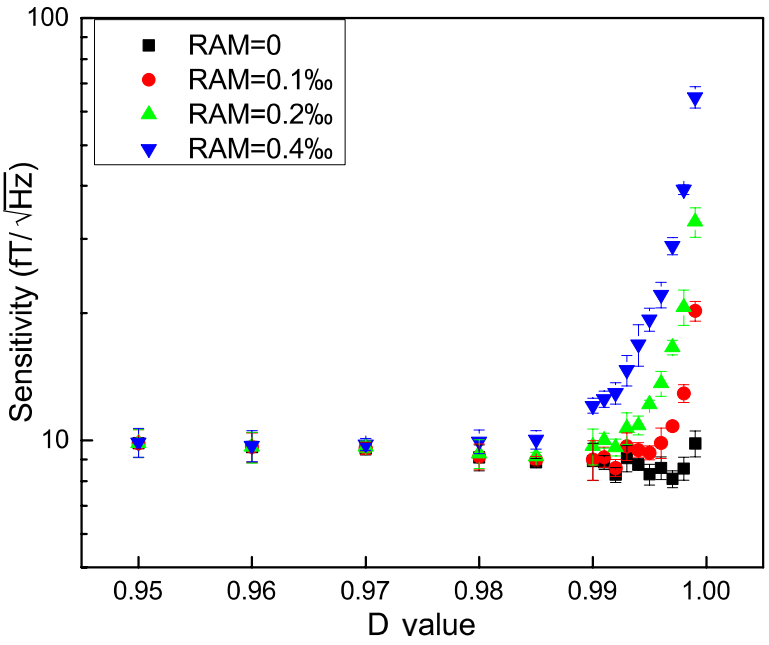

Figure 4 | Dependence of magnetometer sensitivity on the projection parameter *D* under influences of residual amplitude modulation (RAM). Different amounts of common-mode white-intensity-noise were added to the output intensities to mimic RAM. The magnetic field sensitivity was the average sensitivity between 12 Hz and 22 Hz with a properly chosen *D* value to optimize the sensitivity. Experimental parameters are the same as those in Fig. 3 except for the varying *D* values.

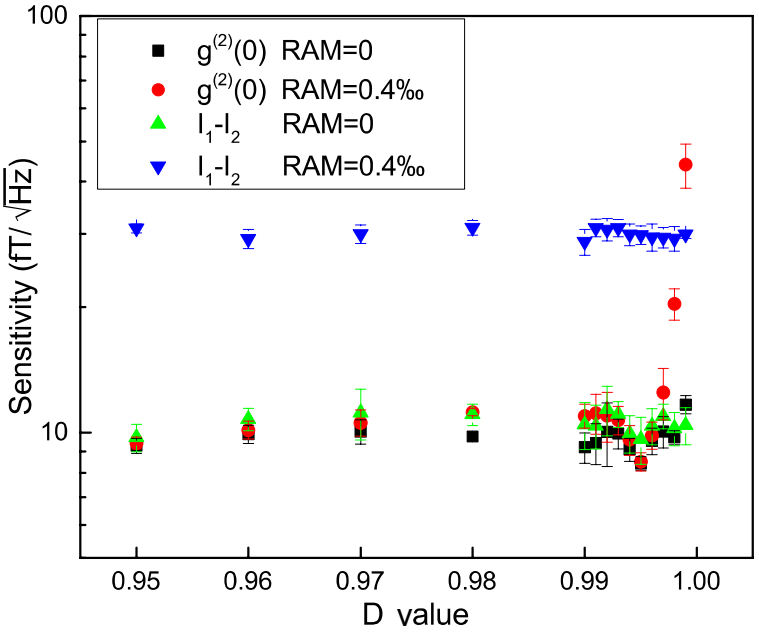

Figure 5 | Comparison of the sensitivities of the WM-$g^{(2)}(0)$ and the intensity-difference technique, with or without RAM for an elliptically-polarized input laser beam. For *D* less than 0.996, the performance of the intensity-difference method is inferior to that of the WM-$g^{(2)}$ method in the presence of RAM. Without RAM, although both methods are comparable in sensitivity, the intensity-difference

method experiences power broadened linewidth of 13 Hz, much wider than that attained by the WM-$g^{(2)}$ process. Experimental parameters: laser input power 15 μW with an ellipticity 1:2.

Methods

Non-Hermitian Hamiltonian for light. By using the atom-light interaction Hamiltonian and solving the master equation, one can obtain the susceptibility for light (see SM). Following the convention that the effective Hamiltonian H for light is written as its wave vector [11][14], we have arrived at the expression for H as in Eq. (1): $H = -i\xi\sigma_z \otimes (|-\omega_m\rangle\langle 0| + |\omega_m\rangle\langle 0|)$, which describes the coupling between the frequency of light ("system") and its polarization ("pointer") denoted by the light Stokes operator σ_z. Here, ω_m is the modulation frequency of the laser, ξ is the small perturbative real-value interaction strength, and $\xi = \frac{\varsigma}{\Gamma}\frac{M}{1+3M^2}\mathrm{Im}[\rho_{cb}]$, with $\varsigma = \frac{n\mu^2}{2\lambda\varepsilon_0\hbar} = \frac{3N\lambda^2}{16\pi^2}\Gamma_0$ and $M = \frac{\lambda_m\omega_m}{\Gamma}$ being the modulation range (λ_m is the modulation depth) normalized to the excited state linewidth Γ, phenomenologically taken as the Doppler broadened width. The imaginary part of the ground-state coherence is $\mathrm{Im}[\rho_{cb}] \simeq \frac{(1+M^2)(1+3M^2)\Gamma_p}{[(1+3M^2)\gamma_2+2(1+M^2)\Gamma_p]^2}\Delta$, at the limit of small Δ ($\ll \Gamma_p$), where Δ is the two-photon detuning proportional to the total magnetic field, and γ_2 is the dephasing rate of the ground-state coherence, and Γ_p represents the optical pumping rate for the ground state, respectively. Other parameters involved above are the following: N is the atomic density, λ is the wavelength of the input laser, and Γ_0 stands for the spontaneous decay rate.

Physically, this optical Hamiltonian H characterizes the differential absorption of the two EIT fields at the modulation frequency ω_m, which is different from previous magnetometers measuring the Faraday rotation angle of a linearly-polarized input laser. Because the system is open and the interaction is non-conservative, these imply H should be non-Hermitian. We note that previous WMs involving light often measure the phase of light, which is associated with a Hermitian optical Hamiltonian [11][14]. On the other hand, the differential absorption at frequency ω_m carries the information of the magnetic field B, since the interaction strength ξ in H is proportional to B. Of importance, if without modulation ($M = 0$) and the laser is on one-photon resonance, the absorption difference between the two EIT fields characterized by σ_z turns out to vanish completely. This explains well why previous atomic magnetometers usually do not measure σ_z, and instead measure σ_y.

Noise correlation $g^{(2)}(0)$ spectroscopy and its relation to σ_z. In our protocol, the key measured quantity is the intensity correlation $g^{(2)}(0) = \langle I_1(t)I_2(t)\rangle_T / \sqrt{\langle I_1^2(t)\rangle_T \langle I_2^2(t)\rangle_T}$, between the two EIT fields' (σ^+ and σ^- components in the laser) output intensities $I_j(t) = E_j^{(-)}(t)E_j^{(+)}(t)$, at the zero-time lag. Here $\langle\cdot\rangle_T$ represents the ensemble average over one modulation period $T = \frac{2\pi}{\omega_m}$. In our WM protocol, the output intensities for the post-selected E_1 and E_2 are, respectively, replaced by $I_1(t) = I_+(t) - D\langle I_+(t)\rangle_T$ and $I_2(t) = I_-(t) - D\langle I_-(t)\rangle_T$ for the σ^+ and σ^- light, where $I_+(t)$ and $I_-(t)$ are the intensities before post-selection. Thanks to the fact that $g^{(2)}(0)$ is bounded between the range of -1 and 1, $\mathcal{L}$ can be deduced by simply seeking the zero-values for the numerator of $g^{(2)}(0)$. Consequently, this is to solve $\left\langle\left[\frac{I_1(t)-I_2(t)}{\langle I_1(t)\rangle_T+\langle I_2(t)\rangle_T}\right]^2\right\rangle_T = 1$. Physics becomes now straightforward if one is aware that the argument is essentially the Stokes parameter $\langle\sigma_z\rangle_{pf}$. Based on this observation, the connection between $\mathcal{L}$

and $\langle\sigma_z\rangle_{pf}$ can be rigorously established via $\frac{I_1(t)-I_2(t)}{\langle I_1(t)\rangle_T+\langle I_2(t)\rangle_T}=\frac{I_+(t)-I_-(t)}{(1-D)(I_+(t)+I_-(t))}=2\langle\sigma_z\rangle_{pf}\times\cos(\omega_m t)$ (see SM). For standard measurements, $\langle\sigma_z\rangle\leq 1$. However, this inequality is in conflict with the condition of $g^{(2)}(0)=0$ which demands $\langle\sigma_z\rangle=\sqrt{2}$. Interestingly, the WV amplification on $\langle\sigma_z\rangle$ solves this problem automatically. After some algebra, one can find the $g^{(2)}(0)$ linewidth to be $\mathcal{L}=\frac{\sqrt{2}}{\left|L\left(\frac{\partial\xi}{\partial\Delta}\right)A_W\right|}$ (see SM), which suggests the anomalous WV-induced narrowing.

The physics of the line narrowing can be also intuitively understood from Fig. 1, where the transmissions of the σ^+ and σ^- components of the input laser are plotted as a function of the one-photon detuning. When the total magnetic field *B* is zero, the two transmission spectra will overlap. However, when *B* is nonzero, they will split with their centers offset by an amount proportional to *B*, resembling the nonlinear Faraday effect. Hence, when the frequency modulation is applied to the laser as shown in the figure, such a modulation is converted to intensity modulations in $\sigma^+$and σ^- light which are anti-correlated due to their opposite slopes on the transmission spectra. For a relatively small *B* as considered in the current work, the slope increases along with the enlarged splitting, giving rise to intensity modulations with a higher amplitude. On the other hand, the correlated part is given by the post-selected DC component (independent of *B*) in intensity. The $g^{(2)}(0)$ value now becomes *B*-dependent since it is determined by the competition between the anti-correlated intensity component and the correlated component. Based on this physics picture, one can now understand that the amplification of the anti-correlated component with respective to the correlated component in intensity makes $g^{(2)}(0)$ cross zero at a smaller detuning, giving rise to a narrowed linewidth. In previously demonstrated $g^{(2)}(0)$ spectroscopy, the DC component was discarded completely and the correlation part was from the AC component at $2\omega_m$ in the intensities which is from a small higher order effect [28] and is hence subject to intensity noises in the laser.

Linewidth and bandwidth. The bandwidth of a magnetometer refers to the range of the frequency of the AC magnetic field that the atoms can sense. Beyond this bandwidth, the dynamics of the atomic states cannot follow the changes of the applied magnetic field. The linewidth of the resonance is related to the system dynamics, and in many cases, it is close to the bandwidth. However, there exist many other factors that can affect the linewidth, such as the measurement scheme and the propagation effects [19]. For example, by measuring $g^{(2)}(0)$, the linewidth of the resonance can be much narrower than that of the bandwidth of the system. Also, when the atomic medium is dense, there is a density narrowing effect on the resonance spectrum [51]. A review on line narrowing mechanisms in EIT can be found in Ref. [52]. Even in absence of these line narrowing effects, the bandwidth can still be different from the linewidth, because the frequency response curve for the atomic magnetometer may not be Lorentzian, although resonance spectra are often Lorentzian. For example, in our case, the EIT linewidth is 13 Hz, mainly determined by the optical pumping rate. However, the frequency response curve follows the form $BW/\sqrt{BW^2+f^2}$ [38] with $BW=16$ Hz, and its HWHM is 28 Hz. This again shows the difference between the linewidth and the bandwidth.

Calibration of magnetic field. We calibrate the magnetic field in two independent ways. In one way, we used a commercial Hall magnetometer to measure the field inside the shield, and obtained a relation between the current in the coil and the *B* field. In the other way, we measure the EIT resonance spectrum either by sweeping the magnetic field (as in this experiment), or by sweeping the frequency difference between the two EIT optical fields controlled by an acoustic-optical-modulator (AOM) (as in Ref. [53]). By comparing the EIT spectra taken under these two ways of varying the two-photon detuning, we can calibrate the Zeeman shift induced by the magnetic field by the frequency of the RF generator, which is used to drive the AOM. Through this procedure, we obtained a reliable conversion between the current in the coil and the applied magnetic field, with a discrepancy less than 10% between these two different calibration methods. This discrepancy, however, does not affect the evaluation of the magnetometer

sensitivity because it contributes to a fixed (non-fluctuating) offset in the absolute value of B.

Sensitivity measurement and noise analysis. To obtain the sensitivity performance in terms of frequency as shown in Fig. 3a, we first apply a small DC magnetic field (with unavoidable noises) which gives $g^{(2)}(0)\sim 0$, corresponding to a relatively large slope on the "$g^{(2)}(0)$ v.s. two-photon detuning" curve. We then record the output intensity fluctuations of the two circular light components for 10 seconds. These fluctuations are mainly distributed around the modulation frequency of 3.03 kHz. One $g^{(2)}(0)$ value can be obtained for each modulation period. Therefore, in 10 seconds, we accumulate 30300 data points of $g^{(2)}(0)$ values fluctuating around zero. Fourier transform is then performed over those 30300 data points, which leads to the noise spectrum of $g^{(2)}(0)$. Next, we measure the $g^{(2)}(0)$ resonance slope for various frequencies of the applied AC magnetic field. Here the slope is defined as the oscillation amplitude of the $g^{(2)}(0)$ value divided by the oscillation amplitude of the applied AC magnetic field. The frequency-response is obtained as in Fig.3b after we normalize the slopes at all frequencies to that at DC. We then divide the above $g^{(2)}(0)$ noise spectrum by the fitted "slope vs. frequency" curve and get the sensitivity spectrum in Fig.3a. The unit conversion to $\mathrm{fT}/\sqrt{\mathrm{Hz}}$ has also been taken care of in the Fourier transform. We note that this is a commonly adopted procedure, also used in [38].

It is worthwhile to point out that though we use a DC magnetic field as the driving field for sensitivity measurement, one can use a different driving frequency. In this case, the sensitivity spectrum in Fig. 3a will remain almost the same except for the appearance of a large peak at the driving frequency [48]. However, if the magnetometer sensitivity is solely limited by the magnetic field noise across the whole spectrum range of interest, the measured sensitivity spectrum will be affected by the noise spectrum of the driving magnetic field.

Since noise is crucial to the magnetometer performance, we have carefully carried out the noise analysis to identify various noise sources in our experiment. By comparing the relative intensity noise at the cell output on and off one-photon resonance, one can determine the photon-shot-noise level, and identify the contribution of laser frequency noise which only gets converted to intensity noise near one-photon resonance. Similarly, the role of the magnetic field noise can be identified by comparing the output intensity noise when EIT is on and off resonance, because the magnetic field noise only couples to the light intensity when on EIT resonance. Our noise analysis shows that, at ~10 Hz, the magnetometer sensitivity is mostly limited by the magnetic field noise from both the environment and the applied field itself. At ~40 Hz, the magnetic field noise slightly decreases and the photon-shot noise starts to play a role in the obtained sensitivity. We note that the magnetic field noise could be eliminated in a gradiometer through multiple-channel operation [38], which is beyond the scope of this paper. Although a coated cell used here is not suitable for gradiometer applications due to motional averaging of the magnetic field across the cell volume, this problem can be solved by using a buffer gas cell or a vacuum cell instead and our WM-$g^{(2)}(0)$ approach still applies.

The spikes appearing in the sensitivity spectrum of Fig. 3a are originated from different mechanisms. The largest spike at 50 Hz is from our ac power line, and the second largest spike at ~23 Hz is due to the vibration of our optics table. Other minor spikes are the results of the electronics noise and magnetic field noise. The sensitivity degradation (Fig. 3a) at higher frequency (above 30 Hz) is due to the effect of the response curve (Fig. 3b), because in this frequency range, a relatively flat shot noise intensity spectrum is obtained. On the other hand, this behavior can be considered as an independent evidence that our magnetometer performance is approaching the fundamental quantum noise limit. In contrast, in Ref. [38], for a similar low frequency range, even though the response curve there is similar to ours, the sensitivity spectrum is more flat because it is all dominated by the magnetic field noise. The photon shot noise limited sensitivity in [38] is considerably below $1\mathrm{fT}/\sqrt{\mathrm{Hz}}$, because the probe laser is of much higher power.

Standard quantum noise limit and quantum backaction noise. Since our magnetometer does not involve any quantum resources such as squeezed light or squeezed atomic spin state, its ultimate sensitivity shall be only limited by the shot noise from either the light or the atoms. For our experimental conditions, the calculated photon shot-noise-limited sensitivity is $3\ \mathrm{fT}/\sqrt{\mathrm{Hz}}$ for the frequency response near 10 Hz, and $6.8\ \mathrm{fT}/\sqrt{\mathrm{Hz}}$ near 40 Hz due to weakened atomic response as shown in Fig. 3b. The estimated atomic shot-noise limit in this system is only $0.2\ \mathrm{fT}/\sqrt{\mathrm{Hz}}$ at DC. Therefore, we are fundamentally limited by photon shot noise, which is because our laser power is relatively weak. In the experiment, the best sensitivity of $7\ \mathrm{fT}/\sqrt{\mathrm{Hz}}$ (in contrast to the quantum limit of $3\ \mathrm{fT}/\sqrt{\mathrm{Hz}}$) was obtained around 10 Hz, limited by the magnetic field noise. Around 40 Hz, because the magnetic field noise slightly decreases, and the shot noise limited sensitivity is slightly worse due to slower atomic response, these two factors become comparable; therefore, the obtained sensitivity of $\sim 10\ \mathrm{fT}/\sqrt{\mathrm{Hz}}$ at 40 Hz (in contrast to the quantum limit of $6.8\ \mathrm{fT}/\sqrt{\mathrm{Hz}}$) is only a factor of 1.5 away from the photon shot-noise limit.

In addition to the normal quantum noise originated from photons or atoms, excess quantum noise may also appear in our system due to the combined resonant atom-light interaction (EIT) and the off-resonant interaction of the EIT fields with other excited state levels, as studied before [48]. Essentially, independent photon shot noises in the two EIT fields randomize the energy difference of the two ground states through AC-stark shift produced by the off-resonant atom-light interaction, and in turn effectively cause excess quantum noise in the *B* measurement. Such noise is also called the backaction noise. As pointed out in Ref. [48], although this process can lead to squeezed light, yet it adversely degrades the polarization rotation measurement in the equator plane of the Poincaré sphere. For instance, the excess quantum noise in the Stokes component σ_y (nearly along the anti-squeezed quadrature of light) can be as large as 10 dB above the photon shot noise [54], indicating a *B* sensitivity 3.3 times worse than the shot noise limit. However, such backaction only enters the relative phase measurement of the two circular light components, and does not affect the intensity measurements as in our protocol. In other words, our protocol measures the polarization rotation along the line of longitude of the Poincaré sphere, which is free from such backaction noise. Though our current experiment does not suffer from this backaction noise appreciably owing to the low optical depth at room temperature, it will become apparent and dominant at higher atomic densities [48]. In such a case, quantum backaction noise has to be taken into account, and our measurement scheme is preferred.

References:

[51] Lukin, M. D., Fleischhauer, M., Zibrov, A. S., Robinson, H. G., Velichansky, V. L., Hollberg, L.& Scully, M. O. Spectroscopy in Dense Coherent Media: Line Narrowing and Interference Effects, *Phys. Rev. Lett.* **79**, 2959 (1997).

[52] Xiao Y. Spectral line narrowing in Electromagnetically Induced Transparency, *Mod. Phys. Lett. B* **23**, 661 (2009).

[53] Peng, P., Cao, W., Shen, C., Qu, W., Wen, J., Jiang, L. & Xiao, Y. Anti-parity-time symmetry with flying Atoms, *Nat. Phys.* **12**, 1139 (2016).

[54] Mikhailov, E., Lezama, A., Noel, T.W. & Novikova, I. Vacuum squeezing via polarization self-rotation and excess noise in hot Rb vapors. *J. Mod. Opt.* **56***,* 1985-1992(2009).